



LAWRENCE
LIVERMORE
NATIONAL
LABORATORY

UCRL-PROC-202356

Including dislocation flux in a continuum crystal plasticity model to produce size scale effects

*A. Arsenlis, R. Becker, D.M. Parks and
V.V. Bulatov*

June 13, 2004

NUMIFORM 2004: The 8th International Conference on
Numerical Methods in Industrial Forming Processes,
The Ohio State University, Columbus, Ohio, USA
June 13-17, 2004

Disclaimer

This document was prepared as an account of work sponsored by an agency of the United States Government. Neither the United States Government nor the University of California nor any of their employees, makes any warranty, express or implied, or assumes any legal liability or responsibility for the accuracy, completeness, or usefulness of any information, apparatus, product, or process disclosed, or represents that its use would not infringe privately owned rights. Reference herein to any specific commercial product, process, or service by trade name, trademark, manufacturer, or otherwise, does not necessarily constitute or imply its endorsement, recommendation, or favoring by the United States Government or the University of California. The views and opinions of authors expressed herein do not necessarily state or reflect those of the United States Government or the University of California, and shall not be used for advertising or product endorsement purposes.

This work was performed under the auspices of the U.S. Department of Energy by University of California, Lawrence Livermore National Laboratory under Contract W-7405-Eng-48.

Including Dislocation Flux in a Continuum Crystal Plasticity Model to Produce Size Scale Effects

Athanasios Arsenlis^{*}, Richard Becker^{*}, David M. Parks^f and Vasily V. Bulatov^{*}

^{*}*University of California, Lawrence Livermore National Laboratory,
7000 East Avenue, P.O. Box 808, Livermore, CA 94551, USA*

^f*Department of Mechanical Engineering, Massachusetts Institute of Technology,
77 Massachusetts Avenue, Cambridge, MA 02139, USA*

Abstract. A novel model has been developed to capture size scale and gradient effects within the context of continuum crystal plasticity by explicitly incorporating details of dislocation transport, coupling dislocation transport to slip, evolving spatial distributions of dislocations consistent with the flux, and capturing the interactions among various dislocation populations. Dislocation flux and density are treated as nodal degrees of freedom in the finite element model, and they are determined as part of the global system of equations. The creation, annihilation and flux of dislocations between elements are related by transport equations. Crystallographic slip is coupled to the dislocation flux and the stress state. The resultant gradients in dislocation density and local lattice rotations are analyzed for geometrically necessary and statistically stored dislocation contents that contribute to strength and hardening. Grain boundaries are treated as surfaces where dislocation flux is restricted depending on the relative orientations of the neighboring grains. Numerical results show different behavior near free surfaces and non-deforming surfaces resulting from differing levels of dislocation transmission. Simulations also show development of dislocation pile-ups at grain boundaries and an increase in flow strength reminiscent of the Hall-Petch model. The dislocation patterns have a characteristic size independent of the numerical discretization.

INTRODUCTION

Plastic deformation of polycrystalline metals results from the motion of dislocations on specific crystallographic slip planes. The dislocations are generated at internal sources, glide through the material, and may be annihilated when they encounter dislocations of opposite character. Interactions of dislocations with each other, with second phase particles, and with grain boundaries, can impede their motion and raise the stress required to move them.

Continuum models of plastic strain in crystals capture deformation by slip on prescribed slip systems. The models don't represent dislocations explicitly; they employ a shear rate representing the average dislocation slip over a unit thickness [1, 2]. Hardening models and kinetic relations have traditionally been phenomenological [2, 3], but recent studies have

employed models that better represent the underlying physics [4-6]. These formulations use dislocation densities on individual slip systems and evolving mean free path lengths as state variables characterizing strain hardening. These models also include generation and annihilation terms to evolve the dislocation density.

A more difficult aspect of dislocation motion to incorporate into a model is the passage of dislocations through the crystal and the coupling of this dislocation flux to the continuum shear rate. Restrictions to dislocation motion imposed by particles, boundaries or gradients in the dislocation field will make slip more difficult and increase the stress required for deformation. This hardening is related to the ease of cross slip and the resistance of barriers, such as grain boundaries, to the passage of dislocations. Such resistance is responsible for the Hall-Petch effect in which strength depends on grain size.

MODEL FORMULATION

The goal of this work is to construct a continuum crystal plasticity model that makes use of a variety of basic dislocation concepts. Further detail is given by Arsenlis, et al. [7]. Some aspects of the model may appear complex or lengthy, but the physical interpretation of the relations is straightforward. The formulation and implementation require tracking dislocation populations on each slip system as well as dislocation fluxes. The relations for generation and annihilation follow the work of Arsenlis and Parks [5].

Crystal Model and Hardening Relations

The crystal plasticity model follows the traditional formulation where the deformation is decomposed into elastic and plastic parts. The elastic part accounts for stretching and rotation of the crystal lattice and the plastic part captures deformation due to slip. Slip occurs along direction \mathbf{m}_0^α on a plane with normal \mathbf{n}_0^α where these directions are defined in the reference configuration. The Greek superscripts denote one of the N slip systems active in the crystal.

In order to track dislocation fluxes through the material and account for differential hardening on the slip systems, it is necessary to carry a representation of the dislocation population in the formulation. Here the dislocations are categorized by their edge or screw character as well as a positive or negative polarity, i.e. ρ_{e+}^α , ρ_{e-}^α , ρ_{s+}^α , ρ_{s-}^α . The edge and screw components are denoted by subscripts e and s , respectively, and subscripted symbols (+) and (-) denote the polarity.

With the dislocation densities resolved into edge and screw components, the plastic shear rate on a slip system is given by

$$\dot{\gamma} = (\rho_{e+}^\alpha \bar{v}_{e+}^\alpha + \rho_{e-}^\alpha \bar{v}_{e-}^\alpha + \rho_{s+}^\alpha \bar{v}_{s+}^\alpha + \rho_{s-}^\alpha \bar{v}_{s-}^\alpha) |\mathbf{b}^\alpha| \quad (1)$$

where \bar{v}^α is the average velocity of the associated dislocation density and \mathbf{b} is the Burgers vector. The sign convention is such that positive dislocation flux quantities result in a positive contribution to a positive shear rate. The velocities are a function of the dislocation state and the applied stress. The particular form is specified in a later section.

The dislocation density within a material volume element evolves through generation and annihilation of dislocations as well as flux into or out of the volume. Dislocation conservation principles require

positive and negative densities to be balanced on generation and annihilation. It is only through passage of dislocations into or out of the volume that an imbalance of positive or negative dislocations can occur.

By considering the geometry of dislocation loops, expressions for the generation of dislocations are postulated to be

$$\begin{aligned} \dot{\rho}_{e+(gen)}^\alpha &= \dot{\rho}_{e-(gen)}^\alpha = \frac{\rho_{s+}^\alpha |\bar{v}_{s+}^\alpha|}{\bar{l}_{s+}^\alpha} + \frac{\rho_{s-}^\alpha |\bar{v}_{s-}^\alpha|}{\bar{l}_{s-}^\alpha} \\ \dot{\rho}_{s+(gen)}^\alpha &= \dot{\rho}_{s-(gen)}^\alpha = \frac{\rho_{e+}^\alpha |\bar{v}_{e+}^\alpha|}{\bar{l}_{e+}^\alpha} + \frac{\rho_{e-}^\alpha |\bar{v}_{e-}^\alpha|}{\bar{l}_{e-}^\alpha} \end{aligned} \quad (2)$$

These relations reflect the creation of edge dislocation length by the motion of screw dislocations and the increase in screw density by the motion of edge dislocations. The \bar{l}^α represent the average length of edge and screw dislocation segments.

The evolution relations for the dislocation segment lengths are based on observations from dislocation dynamics simulations [8]. The equation for the evolution of the average positive edge line length takes the form

$$\begin{aligned} \dot{l}_{e+}^\alpha &= \bar{l}_{e+}^\alpha \frac{\dot{\rho}_{e+}^\alpha}{\rho_{e+}^\alpha} - (\bar{l}_{e+}^\alpha)^3 \times \\ &\quad [H_{ee}^{\alpha\beta} (\dot{\rho}_{e+}^\beta + \dot{\rho}_{e+}^\beta) + H_{es}^{\alpha\beta} (\dot{\rho}_{s+}^\beta + \dot{\rho}_{s+}^\beta)] \end{aligned} \quad (3)$$

The relations for the average negative edge line length and average screw line lengths are similar and are omitted for brevity. The $H_{es}^{\alpha\beta}$ factors are segment-length interaction matrices. In this particular case it accounts for the increase of edge segment length on system α due to screw evolution on system β .

The model for annihilation assumes that dislocations of opposite polarity will combine when they come within a capture radius, R , of each other. This dipole reaction is facilitated by mutual attraction and diffusion, and it will be temperature dependent. The form of the annihilation relations employed here is:

$$\begin{aligned} \dot{\rho}_{e+(ann)}^\alpha &= \dot{\rho}_{e-(ann)}^\alpha = -\rho_{e+}^\alpha \rho_{e-}^\alpha R_e \left(\frac{1}{|\bar{v}_{e+}^\alpha|} + \frac{1}{|\bar{v}_{e-}^\alpha|} \right) \\ \dot{\rho}_{s+(ann)}^\alpha &= \dot{\rho}_{s-(ann)}^\alpha = -\rho_{s+}^\alpha \rho_{s-}^\alpha R_s \left(\frac{1}{|\bar{v}_{s+}^\alpha|} + \frac{1}{|\bar{v}_{s-}^\alpha|} \right) \end{aligned} \quad (4)$$

Dislocation Flux Model

Including the dislocation flux in the model is more involved since advection of the dislocation density requires knowledge of its divergence. As a nonuniform dislocation field moves through a region, the dislocation density at a fixed point in the material will rise and fall. This necessitates including some measure of the dislocation gradient in the formulation. A complete description of this model is given by Arsenlis, et al. [7], and only a brief outline is provided below.

The dislocation population within a finite volume of material can be expressed as a combination of geometrically necessary dislocations (GND) and statistically stored dislocations. However, these labels should not be attached to specific dislocations. GND refers to the imbalance of dislocations of one polarity or another, such as there being more + edge dislocations than – edge dislocations in the volume. They are called geometrically necessary since an abundance of one polarity will result in lattice curvature. In mathematical terms, the GNDs content is described by Nye’s tensor [9] which can be written in terms of the dislocation population as [5]

$$\mathbf{A} \equiv \sum_{\alpha} [(\rho_{e+}^{\alpha} - \rho_{e-}^{\alpha}) \mathbf{b}_0^{\alpha} \otimes \mathbf{p}_0^{\alpha} + (\rho_{s+}^{\alpha} - \rho_{s-}^{\alpha}) \mathbf{b}_0^{\alpha} \otimes \mathbf{m}_0^{\alpha}] \quad (5)$$

where $\mathbf{p}_0^{\alpha} = \mathbf{m}_0^{\alpha} \times \mathbf{n}_0^{\alpha}$ is the tangent line direction to an edge dislocation, and the Burgers vector, \mathbf{b} , is coaxial with \mathbf{m} . The statistically stored dislocations comprise the remainder of the population.

Since the GND content is explicitly connected to lattice curvature, relations can be constructed expressing Nye’s tensor in terms of continuum tensors describing deformation and rotation of the crystal lattice. While several representations have been proposed, here the form advocated by Cermelli and Gurtin [10] is chosen.

$$\mathbf{A} = \text{Curl}(\mathbf{F}^p) \mathbf{F}^{pT} \quad (6)$$

where the derivative involved with the curl operator is in the reference configuration. The GNDs defined in this manner clearly comprise a gradient, and this gradient participates in flux-related changes in dislocation density.

The connection between continuum variables and dislocation content can be made by equating the expressions given for Nye’s tensor in Eqs (5) and (6).

More specifically, a connection between the evolution of dislocations involved in the GNDs and the continuum deformation rate can be obtained by equating the rates of Eqs (5) and (6). This becomes

$$\sum_{\alpha} b_{0(i)}^{\alpha} [(\dot{\rho}_{e+}^{\alpha} - \dot{\rho}_{e-}^{\alpha}) p_{0(q)}^{\alpha} + (\dot{\rho}_{s+}^{\alpha} - \dot{\rho}_{s-}^{\alpha}) m_{0(q)}^{\alpha}] \quad (7)$$

$$= e_{pj k} \frac{\partial L_{il}^p}{\partial X_k} F_{lj}^p F_{qp}^p + L_{il}^p A_{lq} + A_{il} L_{qt}^p$$

These dislocation evolution rates are associated with the dislocation flux, but it is important to note that the fluxes cannot be uniquely determined from this relation. Only the differences are prescribed. An increase in dislocations of one sense cannot be distinguished from loss of dislocations of the opposite sense. In addition, an equal flux of positive and negative sense dislocations is not captured.

By appealing to certain physical considerations, a possible set of evolution equations may be developed by assuming that the polarity of the dislocation density in a given slip system results from processes involving dislocation densities within the slip system. Rewriting \mathbf{L}^p in terms of crystallographic dislocation densities,

$$\mathbf{L}^p = \sum_{\alpha} \dot{\gamma}^{\alpha} \mathbf{m}_0^{\alpha} \otimes \mathbf{n}_0^{\alpha} \quad (8)$$

with $\dot{\gamma}^{\alpha}$ given by Eq (1), and separating the contributions of each of the dislocation densities, the proposed form for the positive edge and screw density evolution rates due to dislocation flux are, respectively

$$\dot{\rho}_{e+(flux)}^{\alpha} = -\frac{\partial}{\partial \mathbf{X}} [\rho_{e+}^{\alpha} \bar{\mathbf{v}}_{e+}^{\alpha} + f_e (\rho_{s+}^{\alpha} \bar{\mathbf{v}}_{s+}^{\alpha} - \rho_{s-}^{\alpha} \bar{\mathbf{v}}_{s-}^{\alpha})] \cdot \mathbf{F}^{p-1} \cdot \mathbf{m}_0^{\alpha} \quad (9)$$

$$+ [\rho_{e+}^{\alpha} \bar{\mathbf{v}}_{e+}^{\alpha} + f_e (\rho_{s+}^{\alpha} \bar{\mathbf{v}}_{s+}^{\alpha} - \rho_{s-}^{\alpha} \bar{\mathbf{v}}_{s-}^{\alpha})] \mathbf{n}_0^{\alpha} \cdot \mathbf{A} \cdot \mathbf{p}_0^{\alpha}$$

$$+ \rho_{e+}^{\alpha} \mathbf{p}_0^{\alpha} \cdot \mathbf{L}^p \cdot \mathbf{p}_0^{\alpha} + f_e (\rho_{s+}^{\alpha} - \rho_{s-}^{\alpha}) \mathbf{p}_0^{\alpha} \cdot \mathbf{L}^p \cdot \mathbf{m}_0^{\alpha}$$

and

$$\dot{\rho}_{s+(flux)}^{\alpha} = -\frac{\partial}{\partial \mathbf{X}} [\rho_{s+}^{\alpha} \bar{\mathbf{v}}_{s+}^{\alpha} + f_s (\rho_{e+}^{\alpha} \bar{\mathbf{v}}_{e+}^{\alpha} - \rho_{e-}^{\alpha} \bar{\mathbf{v}}_{e-}^{\alpha})] \cdot \mathbf{F}^{p-1} \cdot \mathbf{p}_0^{\alpha} \quad (10)$$

$$+ [\rho_{s+}^{\alpha} \bar{\mathbf{v}}_{s+}^{\alpha} + f_s (\rho_{e+}^{\alpha} \bar{\mathbf{v}}_{e+}^{\alpha} - \rho_{e-}^{\alpha} \bar{\mathbf{v}}_{e-}^{\alpha})] \mathbf{n}_0^{\alpha} \cdot \mathbf{A} \cdot \mathbf{m}_0^{\alpha}$$

$$+ \rho_{s+}^{\alpha} \mathbf{m}_0^{\alpha} \cdot \mathbf{L}^p \cdot \mathbf{m}_0^{\alpha} + f_s (\rho_{e+}^{\alpha} - \rho_{e-}^{\alpha}) \mathbf{m}_0^{\alpha} \cdot \mathbf{L}^p \cdot \mathbf{p}_0^{\alpha}$$

f_e and f_s in Eqs (9) and (10) are dimensionless functions with properties

$$\begin{aligned}
0 \leq f_e(\rho_{e+}^\alpha, \rho_{e-}^\alpha) \leq 1, \quad f_e(\rho_{e+}^\alpha = 0, \rho_{e-}^\alpha) &= 0 \\
f_e(\rho_{e+}^\alpha, \rho_{e-}^\alpha = 0) &= 1, \quad f_e(\rho_{e+}^\alpha = \rho_{e-}^\alpha, \rho_{e-}^\alpha) = \frac{1}{2} \quad (11) \\
0 \leq f_s(\rho_{s+}^\alpha, \rho_{s-}^\alpha) \leq 1, \quad f_s(\rho_{s+}^\alpha = 0, \rho_{s-}^\alpha) &= 0 \\
f_s(\rho_{s+}^\alpha, \rho_{s-}^\alpha = 0) &= 1, \quad f_s(\rho_{s+}^\alpha = \rho_{s-}^\alpha, \rho_{s-}^\alpha) = \frac{1}{2}
\end{aligned}$$

The dislocation density evolution rate due to negative edge and screw fluxes are similar to Eqs (9) and (10) with some sign changes and f replaced by $(I-f)$ [7].

In addition to the edge and screw density increases due to dislocation flux, there is also an increase in jog density. The jog density has not been explicitly incorporated into the model at this point, mainly because climb of edge dislocation has been ignored and the density of jogs formed by statistical interactions of gliding densities is assumed to be much lower than the edge and screw densities.

The terms in the proposed density flux equations can be interpreted in terms of physical processes. The first term is a flux gradient in the direction of motion of the dislocation line segments. This is the imbalance of dislocations entering and leaving the volume on that slip plane. The first term in the square brackets is the average edge dislocation flux. The remaining quantities in the square brackets create edge and screw kink density.

The second term of Eqs (9) and (10) has the same quantity in square brackets as the first, but it is multiplied by a geometric factor related to lattice curvature and GNDs. This accounts for an imbalance of dislocations entering or leaving the volume due to curvature of the lattice. If the lattice is straight and dislocation flux uniform, equal amounts of density enter and leave the volume. If, however, the lattice is curved, there may be an imbalance of dislocations entering and leaving the volume.

The final two terms of Eqs (9) and (10) deal with changed in dislocation density related to configuration changes. The third term adds density as the lines are stretched. The final term is similar but related to distortion of the volume.

FINITE ELEMENT IMPLEMENTATION

Implementation of the equilibrium equations in a finite element code is common and will not be

discussed here. Taken by themselves, the dislocation density evolution equations resulting from generation and annihilation can be integrated as material state variables in a local constitutive model. Inclusion of the flux gradient terms complicates the implementation. The density evolution involves gradients and cannot be treated as a local constitutive model. The dislocation densities are identified as nodal variables to achieve continuity of density from element to element and to permit gradient calculations. The densities are treated as unknowns to be determined, along with the nodal displacements, from a global system of equations.

The discussion will focus on equations for the positive edge dislocation density. The treatment is applicable to the other density components. Begin with a relation for the density evolution of the form

$$0 = \dot{\rho}_{e+}^\alpha - \left(\dot{\rho}_{e+(gen)}^\alpha + \dot{\rho}_{e+(ann)}^\alpha + \dot{\rho}_{e+(flux)}^\alpha \right) \quad (12)$$

where the terms in parentheses are to be substituted from Eqs (2), (4) and (9).

Motivated by Galerkin formulations, Eq (12) is multiplied by a virtual density, $\tilde{\rho}$, and integrated over the volume. The resulting equations cannot be easily integrated since the average dislocation velocities are not nodal variables that can be readily interpolated or differentiated. By using the Divergence Theorem, the spatial derivatives are transferred to the virtual density, yielding a final weak form for the equations.

The resulting equations can be implemented within a finite element framework, and the constitutive functions specified can be evaluated at numerical quadrature points. In this weak form, the GND related terms are integrated without calculating derivatives of the dislocation flux or gradients in the plastic strain rate. Also evident from these equations is that additional boundary conditions are needed to properly specify the problem when a polarity in the dislocation density is considered. A detailed discussion of these conditions, their implications, and the implementation of the model as a user-defined element in ABAQUS is given by Arsenlis, et al. [7].

Dislocation density/density-flux conditions must be applied at the boundaries to solve the density evolution equations. A density-flux condition may be imposed at a boundary to set the rate of plastic deformation associated with that slip system. A zero density-flux condition, with a non-zero dislocation density, is equivalent to placing an impenetrable wall at the boundary. At a free boundary there is no impediment to dislocation flux. The dislocation density at the surface can also be prescribed. For example,

dislocations leave free surfaces due to image forces, so a free surface can act as a dislocation sink. In the extreme limit with infinite dislocation mobility, a free surface would have a zero dislocation density. The examples cited below use the two extremes of an impenetrable surface with zero dislocation flux imposed and a free surface with a zero dislocation density prescribed.

EXAMPLES

To illustrate the behavior of the model, a series of finite element simulations are conducted on a simplified geometry using a two-dimensional, plane-strain idealization of a single crystal. The simulations are of simple shear applied to a single crystal. The height (y -direction) of the crystal is normal to the shearing direction, and it is varied between $3\ \mu\text{m}$ and $300\ \mu\text{m}$ to illustrate length scale effects. The width (x -direction) of the crystal is in the shearing direction, and it is considered to be infinite. Periodic displacement boundary conditions are used in the x -direction. The displacements on the bottom of the crystal at $y=0$ are constrained. The upper surface is constrained from motion in the y -direction and displaced in the positive x -direction to apply the simple shear loading.

The simplified crystal geometry consists of a single slip system oriented with the slip plane normal in the x -direction and the slip direction along the y -axis. The configuration resembles a deck of cards stood on end and sheared by moving the top parallel to the table surface. This geometry supports three dislocation densities: a positive and a negative edge density and a screw dipole density. The two-dimensional geometry restricts the screw density to be non-polar.

The kinetic model prescribing the average dislocation velocities in terms of the resolved shear stress and a dislocation-dependent strength is taken to be

$$\bar{v}_{e+} = \bar{v}_{e-} = \bar{v}_s = v_0 \left(\frac{|\mathbf{m}_0 \cdot \mathbf{T} \cdot \mathbf{n}_0 - B|}{c\mu|\mathbf{b}|\sqrt{\rho_{e+} + \rho_{e-} + \rho_s}} \right)^{\frac{1}{m}} \times \text{sign}(\mathbf{m}_0^\alpha \cdot \mathbf{T} \cdot \mathbf{n}_0^\alpha - B) \quad (13)$$

$$B = a\mu|\mathbf{b}| \frac{\mathbf{m}_0 \cdot \mathbf{F}^{p-1} \cdot \text{Grad}(\rho_{e+} - \rho_{e-})}{\rho_{e+} + \rho_{e-}} \quad (14)$$

Thus, the gradient in dislocation density enters through the hardening relation as well as the direct coupling to the plastic velocity gradient.

The boundary conditions applied to the density/density-flux at the upper and lower surfaces represent the extremes of an impenetrable barrier and a free surface acting as a strong dislocation sink.

Results from calculations with the dislocation flux constrained at the surfaces are shown in Figs 1 and 2. Figure 1 gives contours of accumulated slip on the deformed geometries of five different height crystals to an average shear strain of 0.05. The restrictions on the dislocation flux impede slip at the top and bottom surfaces. This results in the noticeable strain gradient in the $3\ \mu\text{m}$ thick crystal. The constraint is based on a gradient in dislocation density, so it decays within a physical length scale. Hence, as the crystal size increases, the effect of the constraint is confined to a smaller fraction of the overall crystal height. The $300\ \mu\text{m}$ case has nearly uniform shear through the thickness. The result of that simulation is similar to the prediction without the flux terms included.

Figure 2 shows the shear stress-shear strain curves for these five simulations. For the thicker cases the gradient at the boundary affects only a small portion of the total region modeled and the influence of the flux boundary conditions is minimal. As the thickness decreases, the effect of the boundary constraint becomes dominant and the stress required to deform the crystals increases.

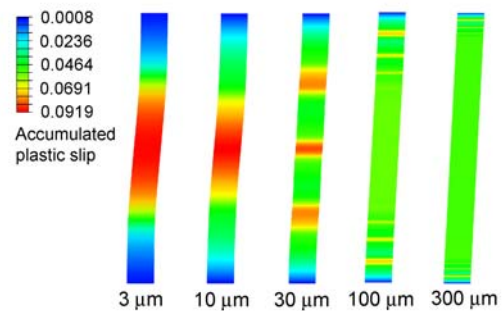


FIGURE 1. Contours of slip for sheared films with the surface dislocation flux constrained. The labels beneath each figure denote their height.

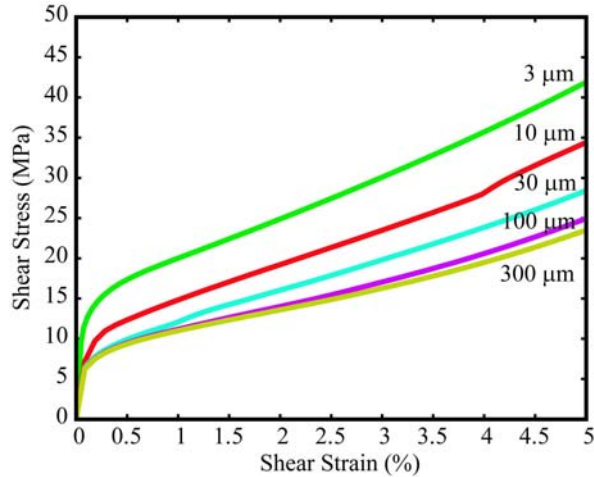


FIGURE 2. Contours of slip for sheared films with the surface dislocation flux constrained.

Results from calculations using the boundary condition at the other extreme are shown in Figs 3 and 4. Here the surfaces act as a sink for dislocations. Figure 3 gives contours of accumulated slip on the deformed geometry for the same five thicknesses that were used in the previous simulations. Unlike the previous examples, here greater shear occurs near the ends for the thinner specimens. The boundary condition depletes the dislocation population and, according to Eq (13), lowers the resistance to shear. As the thickness increases, the effect is confined to a smaller and smaller fraction of the overall height, similar to the constrained flux boundary condition.

The shear stress-shear strain curves for these calculations are shown in Fig. 4. Unlike the constrained end conditions, the response shows little size dependence.

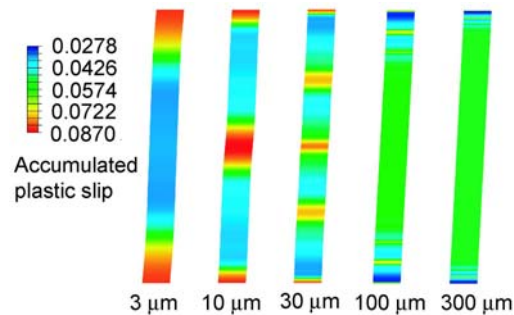


FIGURE 3. Contours of slip for sheared films with a free surface boundary condition acting as a dislocation sink. The labels beneath each figure denote their height.

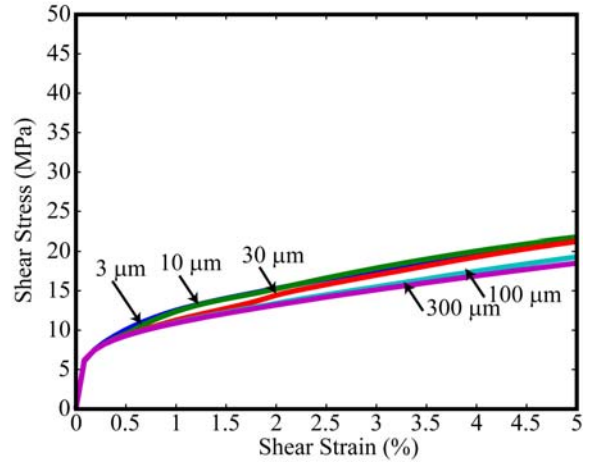


FIGURE 4. Contours of slip for sheared films with a free surface boundary condition acting as a dislocation sink.

ACKNOWLEDGMENTS

This work was performed under the auspices of the U.S. Department of Energy by the University of California, Lawrence Livermore National Laboratory under Contract No. W-7405-Eng-48. Additional support was provided by the National Defense and Engineering Graduate Fellowship Program and by the National Science Foundation, Grant No. 9700358.

REFERENCES

- Asaro, R.J. and Rice, J.R., *J. Mech. Phys. Solids* **25**, 309-338 (1977).
- Peirce, D.J., Asaro, R.J. and Needleman, A., *Acta Metall.* **31**, 1951-1976 (1983).
- Becker, R., *Acta Mater.* **46**, 1385-1401 (1998).
- Cuitino, A.M. and Ortiz, M., *Modell. Simul. Mater. Sci. Engr.* **1**, 225-263 (1992).
- Arsenlis, A. and Parks, D.M., *Acta Mater.* **47**, 1597-1611 (1999).
- Stainier, L., Cuitino, A.M. and Ortiz, M., *J. Mech. Phys. Solids* **50**, 1511-1545 (2002).
- Arsenlis, A., Parks, D.M., Becker, R. and Bulatov, V.V., *J. Mech. Phys. Solids*, to appear (2004).
- Arsenlis, A. and Tang, M., *Modell. Simul. Mater. Sci. Engr.* **11**, 251-264 (2003).
- Nye, J.F., *Acta Metall.* **1**, 153-162 (1953).
- Cermelli, P. and Gurtin, M.E., *J. Mech. Phys. Solids* **49**, 1539-1568 (2001).